

## Quantum simulations of the hydrogen molecule on ammonia clusters

Massimo Mella and E. Curotto

Citation: *J. Chem. Phys.* **139**, 124319 (2013); doi: 10.1063/1.4821648

View online: <http://dx.doi.org/10.1063/1.4821648>

View Table of Contents: <http://jcp.aip.org/resource/1/JCPSA6/v139/i12>

Published by the AIP Publishing LLC.

---

### Additional information on J. Chem. Phys.

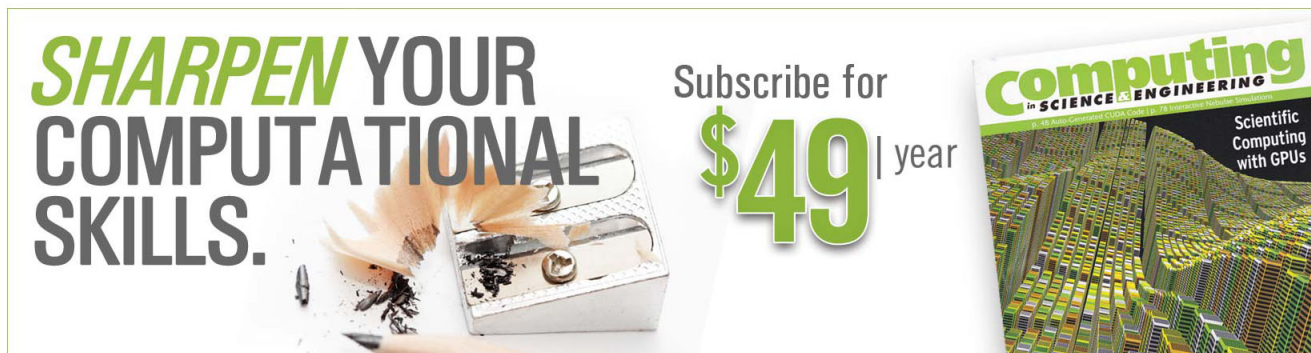
Journal Homepage: <http://jcp.aip.org/>

Journal Information: [http://jcp.aip.org/about/about\\_the\\_journal](http://jcp.aip.org/about/about_the_journal)

Top downloads: [http://jcp.aip.org/features/most\\_downloaded](http://jcp.aip.org/features/most_downloaded)

Information for Authors: <http://jcp.aip.org/authors>

## ADVERTISEMENT



**SHARPEN YOUR  
COMPUTATIONAL  
SKILLS.**

Subscribe for  
**\$49** | year

**computing**  
in SCIENCE & ENGINEERING  
Scientific  
Computing  
with GPUs

## Quantum simulations of the hydrogen molecule on ammonia clusters

Massimo Mella<sup>1,a)</sup> and E. Curotto<sup>2,b)</sup>

<sup>1</sup>*Dipartimento di Scienze ed Alta Tecnologia, Università degli Studi dell'Insubria, via Valleggio 11, 22100 Como, Italy*

<sup>2</sup>*Department of Chemistry and Physics, Arcadia University, Glenside, Pennsylvania 19038–3295, USA*

(Received 8 May 2013; accepted 5 September 2013; published online 30 September 2013)

Mixed ammonia–hydrogen molecule clusters  $[H_2-(NH_3)_n]$  have been studied with the aim of exploring the quantitative importance of the  $H_2$  quantum motion in defining their structure and energetics. Minimum energy structures have been obtained employing genetic algorithm-based optimization methods in conjunction with accurate pair potentials for  $NH_3-NH_3$  and  $H_2-NH_3$ . These include both a full 5D potential and a spherically averaged reduced surface mimicking the presence of a *para*- $H_2$ . All the putative global minima for  $n \geq 7$  are characterized by  $H_2$  being adsorbed onto a rhomboidal ammonia tetramer motif formed by two double donor and two double acceptor ammonia molecules. In a few cases, the choice of specific rhombus seems to be directed by the vicinity of an ammonia ad-molecule. Diffusion Monte Carlo simulations on a subset of the species obtained highlighted important quantum effects in defining the  $H_2$  surface distribution, often resulting in populating rhomboidal sites different from the global minimum one, and showing a compelling correlation between local geometrical features and the relative stability of surface  $H_2$ . Clathrate-like species have also been studied and suggested to be metastable over a broad range of conditions if formed. © 2013 AIP Publishing LLC. [<http://dx.doi.org/10.1063/1.4821648>]

### I. INTRODUCTION

Weak interactions between adsorbed molecules and solid surfaces, including the ones inside nano-pores or nanocavities, are at the heart of many possible scientific interests and applications. For instance, spectroscopically studying both the surface and adsorbed species may allow a more detailed characterization of the surface structure and how the latter facilitates or induces specific reactions. As typical examples, there are the studies on molecular adsorption on water ice, with  $H_2$ <sup>1–8</sup> and  $HX$  ( $X = Cl, Br$ )<sup>9–17</sup> being perhaps the most studied ad-species. Ammonia<sup>18</sup> and small hydrocarbons<sup>19</sup> have also been studied for their peculiarity or relevance. In a few cases, the thrust behind this effort has been provided by the need for modeling processes in the interstellar medium<sup>20–23</sup> or in regions of earth atmosphere.<sup>24–26</sup>

Weak surface-small molecule interactions are also fundamental in separation science. For example, isotopic separation can be achieved exploiting a chromatographic-like approach based on differences in binding energy induced by nuclear spin statistics,<sup>2,3,5,27</sup> or intermolecular forces.<sup>28,29</sup> Interestingly, separation can be kinetically achieved exploiting the coupling between quantum translational and rotational motions.<sup>30–33</sup> In the latter case, the effect is magnified by small pores and leads to a ramping up of the selectivity to a ratio of 50:1 for the pair  $T_2/H_2$ .<sup>31</sup>

Weak interactions between gases and nano- or porous materials also bear relevance to the development of gas storage methods employing mild conditions, the latter requirement being particularly important for the development of

hydrogen fuel economy and the safe transportation of dangerous gasses. Whether inside metal organic frameworks (MOF)<sup>28,34,35</sup> or in clathrates,<sup>36–39</sup> the stored gas must be trapped in liquid or solid phases tuning the balance between the gas–gas and the gas–surface interactions. Thus, material–gas forces must be sufficiently strong to nearly freeze one or a few gas layers, therefore eliminating the size-dependent change in melting and boiling points well known in cluster physics.<sup>40,41</sup>

Different from the driving forces that guide the formation of solid materials (see, e.g., the MOF case<sup>42</sup>), the fundamental rules that govern the effects of the interaction between gas molecules and material surfaces are far less clear despite a few obvious guidelines based on gas molecular properties.<sup>28</sup> This is especially true for quantum species such as  $H_2$  and its isotopomers,<sup>43</sup> which require an appropriate treatment for several juxtaposing effects.<sup>2,3,5,27,30–33,37,38,44</sup> In the context just presented, we thus consider interesting to investigate the structure and energetics of small and medium sized  $H_2-(NH_3)_n$  aggregates. Apart from the lack of basic information on these systems, which include the general study of the importance of quantum effects in describing molecular aggregates, there are several interconnected and directly supporting motivations for applying ourselves to this task:

1. Ammonia ice micro-grains compose clouds in the atmosphere of several planets and satellites<sup>45–47</sup> providing the mechanical support for chemical reactions involving molecular species of several kind (among which  $H_2$ ).
2. Radiation damage of ammonia ice<sup>48,49</sup> may be a direct source of molecular hydrogen as it is methane ice dust,<sup>50</sup> a product that can be thermalized and adsorbed on the surface.

<sup>a)</sup> Author to whom correspondence should be addressed. Electronic mail: [massimo.mella@uninsubria.it](mailto:massimo.mella@uninsubria.it)

<sup>b)</sup> [curottom@arcadia.edu](mailto:curottom@arcadia.edu)

3. Hydrogen atoms may recombine into H<sub>2</sub> on the surface of ammonia ice, a common species in interstellar space, as it happens on water ice,<sup>51,52</sup> the detailed understanding of the possible mechanism requiring energetics details.<sup>53</sup>
4. Condensed mixtures of ammonia and hydrogen molecules, whether as clathrates or “slush,” may be useful for automotive transportation employing ammonia fueled engines.
5. Since H<sub>2</sub> adsorption properties of ammonia ice would depend on its surface or micropore morphology as it happens for water ice,<sup>2,3</sup> a better understanding of the adsorption energy as a function of the surface structural motifs would be useful in interpreting possible experiments.
6. H<sub>2</sub> tagging can be used as a useful probe of local structure if the substrate–H<sub>2</sub> binding energy is of the correct order of magnitude;<sup>54</sup> forming mixed H<sub>2</sub>–NH<sub>3</sub> species in cold environment may thus help elucidating the structural details of ammonia clusters formed in gas phase<sup>55–58</sup> and He droplets.<sup>59,60</sup>

Given the items discussed above, the explicit aims of the present work are exploring (a) the possible structural effects of adding a H<sub>2</sub> molecule to a (NH<sub>3</sub>)<sub>n</sub>, if any, (b) the binding sites on the cluster surface to understand the relationship between the local features and adsorption binding energy, and (c) the quantum effects intrinsically associated with the librational motion of adsorbed H<sub>2</sub>. The latter can, in fact, modify the classical energy landscape.

As the interaction energy between the hydrogen and ammonia molecules is rather small in magnitude compared with the one between two ammonia molecules,<sup>61–63</sup> it has a negligible influence on the internal structure of NH<sub>3</sub> and H<sub>2</sub>.<sup>63</sup> This ought to be true also for the structure of ammonia clusters, which are held together by stronger intermolecular forces than between H<sub>2</sub> and ammonia. It is however possible that the energy landscape of the mixed clusters does not closely follow the one for the pure species, the chance of reordering being high in our case since the pure systems may present nearly degenerate isomers (*vide infra* Secs. II B and III A) as suggested in Ref. 64. Thus, our work starts with an extensive search of putative global minima from preformed (NH<sub>3</sub>)<sub>n</sub> aggregates ( $n = 3 - 20$ ) over which H<sub>2</sub> lands. This search is conducted using a fully dimensional (i.e., 5D) rigid-rotor potential energy surface (PES) and its 3D counterpart, spherically averaged over the orientation of H<sub>2</sub>.<sup>63</sup> A selected subset of clusters is subsequently simulated to investigate possible quantum effects. A “vis á vis” comparison of the classical and quantum results coming from the two PESs would also aid in assessing the shortcomings introduced by the spherical average from the quantitative viewpoint.<sup>65</sup>

## II. METHODS

### A. Potential energy surfaces

As customary with these kinds of studies, we employ a pairwise potential to describe the interaction between the ammonia molecules and the single H<sub>2</sub> molecule in our species.

Specifically, we opted for using the PES recently developed by us on the basis of MP4 calculations,<sup>63</sup> for which a full 5D treatment of the rigid hydrogen molecule, and a rotationally averaged 3D version (i.e., assuming uniform spatial orientation for the *para*-H<sub>2</sub>) are readily available. As to the 3D surface, it is worth mentioning that it represents a point-wise approximation of the true interaction when it is assumed that the rotational motion of an interacting H<sub>2</sub> is identical to its free-rotor (i.e., non-interacting and decoupled) counterpart at any location of its center of mass with respect to NH<sub>3</sub>. The effect of such approximation has recently become better quantified,<sup>66</sup> so that its impact on the quantum treatment of the remaining (vibrational) degrees of freedom is now recognized to be in the range of a few cm<sup>-1</sup>.

The 5D model is built as a sum of four sources for electrostatic, dispersion, and repulsion interactions on ammonia and one on the hydrogen molecule, each source being described with a short multipolar expansion whose terms are weighted by distance depending exponential terms. The choice of a pairwise model is in this case justified by the low polarizability of the hydrogen molecule ( $\alpha_{\parallel} = 6.383$  and  $\alpha_{\perp} = 4.577$  a.u.<sup>67</sup>), and thus by the expected small impact of a self-consistent description of the induction approach.<sup>68</sup> However, the direct polarization term is effectively introduced by means of the multipolar expansion employed to describe the electrostatic component of the surface. The 5D analytical surface<sup>63</sup> presents a global minimum geometry with the hydrogen molecule aligned to the ammonia C<sub>3</sub> axis and on the side of the nitrogen, with a D<sub>e</sub> of roughly 0.7 kcal/mol (245 cm<sup>-1</sup>). A second minimum (D<sub>e</sub> ~ 0.26 kcal/mol or 92.0 cm<sup>-1</sup>) is also found on the H-side of ammonia, with the center of mass of H<sub>2</sub> along a N–H vector and its bond axis being nearly perpendicular to the latter. Upon reducing the dimensionality of the PES by averaging over a uniform distribution for the spherical angles (i.e., assuming decoupling between rotational and intermolecular vibrational motions for *para*-H<sub>2</sub>), the energetic ordering is inverted. In fact, the minimum along the N–H vector has a D<sub>e</sub> ~ 0.18 kcal/mol (63.4 cm<sup>-1</sup>), while the one along the C<sub>3</sub> axis on the N-side has a D<sub>e</sub> ~ 0.08 kcal/mol (23.7 cm<sup>-1</sup>). It is also worth remembering that there is another minimum for *para*-H<sub>2</sub> along the C<sub>3</sub> axis and located on the H-side with D<sub>e</sub> = 0.081 kcal/mol (28.3 cm<sup>-1</sup>). From the data mentioned, it therefore appears that the stronger quadrupole–dipole interaction between the H atoms in H<sub>2</sub> and the nitrogen accounted for by the 5D surface is effectively “washed out” by the rotational average.

To describe the interaction between ammonia molecules, we employed a rigid model including point charges, dispersion, and repulsion terms on *all* atoms, as well as an induction term based on a single-step “charge on spring” (CoS) model.<sup>64,69</sup> This PES, parameterized against extensive MP2 calculations, has been used previously to study both the energetics<sup>64,70,71</sup> and isomer formation probabilities<sup>60</sup> of medium sized (NH<sub>3</sub>)<sub>n</sub>. When compared to BSSE-corrected MP2/aug-cc-pVTZ calculation,<sup>72</sup> the polarizable interaction model appeared capable of correctly predicting the trend in binding energy and global minimum structure as a function of the number of ammonia molecules for (NH<sub>3</sub>)<sub>n</sub> ( $n = 2-5$ ). It also demonstrated the capability of correctly suggesting the

presence of high lying minima never studied previously for  $n = 5$  and 6.<sup>60</sup> For the sake of the ensuing discussion, we mention that  $V_{\text{NH}_3}(\mathbf{Y}_1, \dots, \mathbf{Y}_n)$  predicts a fragmentation energy  $D_e \sim 2.85$  and 9.06 kcal/mol for the ammonia dimer and trimer, respectively. A *vis à vis* comparison between these two values clearly indicates the substantial many-body nature engendered by the single-step CoS induction term.

Employing the aforementioned models, the PES for a general  $\text{H}_2\text{-(NH}_3)_n$  system ought to be written as

$$V(\mathbf{Y}_1, \dots, \mathbf{Y}_n, \mathbf{Y}_{\text{H}_2}) = V_{\text{NH}_3}(\mathbf{Y}_1, \dots, \mathbf{Y}_n) + \sum_{i=1}^n V_{\text{H}_2\text{-NH}_3}(\mathbf{Y}_i, \mathbf{Y}_{\text{H}_2}), \quad (1)$$

where  $V_{\text{NH}_3}(\mathbf{Y}_1, \dots, \mathbf{Y}_n)$  is the interaction potential between *all* the ammonia molecules,  $V_{\text{H}_2\text{-NH}_3}(\mathbf{Y}_i, \mathbf{Y}_{\text{H}_2})$  is the potential between the hydrogen molecule and the  $i$ th ammonia molecule,  $\mathbf{Y}_i \equiv (x_i, y_i, z_i, \alpha_i, \beta_i, \gamma_i)$  and  $\mathbf{Y}_{\text{H}_2} \equiv (x_{\text{H}_2}, y_{\text{H}_2}, z_{\text{H}_2}, \phi, \theta)$ . Here, the Cartesian coordinates indicate the position of the molecular center of mass, while the Euler or polar angles describe the molecular orientation with respect to the laboratory frame. Importantly, the pairwise nature of the ammonia–hydrogen surface, and the single-step CoS model for induction in  $V_{\text{NH}_3}(\mathbf{Y}_1, \dots, \mathbf{Y}_n)$  allow one to analytically derive the force vector, which is needed for the energy minimization employed during the search for putative global minima as a function of  $n$  (*vide infra* Sec. II B).

## B. Energy minimization

The structures and energies of the minima for the pure ammonia clusters  $(\text{NH}_3)_{2-20}$  have been determined in our previous studies.<sup>64,70</sup> However, the complexity of the potential energy surface for the  $\text{NH}_3\text{-NH}_3$  interaction creates challenges for the traditional implementation of the genetic algorithm.<sup>73-77</sup> The typical 40 generation with 100 children for generation employed on the dodecamer, for example, is not sufficient to find the second minimum we had obtained in our earlier work.<sup>70</sup> Therefore, before attempting to minimize the full system in Eq. (1), we rerun a parallelized version of the genetic algorithm on the pure ammonia clusters  $(\text{NH}_3)_{2-20}$ , so that 11 000 children are created and minimized for every generation. Two parents are selected using the lowest energy criteria as best fitness, and the children are created using a two point crossover operator.<sup>76</sup>

We use  $T = 0$  Brownian dynamics to minimize the children using finite differences to estimate the gradient of the Lagrangian as we did in earlier work,<sup>64</sup> and we end the Brownian trajectory when the size of the potential energy gradient is smaller than one part in  $10^7$ . Notice that at  $T = 0$  there is no stochastic component in the dynamics, making it similar to the steepest descent method with a fixed fractional step-length; thus, the only advantage that comes from the approach used by us for the minimization is related to code availability. Each set of children is added to the pool of parent structures, compared structurally, sorted energetically, and the bottom 100 distinct minima in this new list become the parent structures for the new generation. We terminate the search when successive generations yield the same lowest 100 energy

TABLE I. Potential energy  $V_0^d$  for the  $\text{H}_2\text{-(NH}_3)_n$  putative global minimum, the vertical  $\text{H}_2$  binding energy  $D_v$ , the  $\text{H}_2$  binding energy  $D_e$  with respect to the parent  $(\text{NH}_3)_n$ , and the relaxation energy  $\Delta_r$  of  $(\text{NH}_3)_n$  from the structure in the optimal  $\text{H}_2\text{-(NH}_3)_n$  to its closest minimum. Data obtained using the full 5D PES for  $\text{H}_2\text{-NH}_3$ , in  $\text{cm}^{-1}$ .

$n$	$V_0^d$	$D_v$	$D_e$	$\Delta_r$
3	-3956.01	-685.21	-661.58	23.63
4	-6059.90	-690.13	-641.95	48.18
5	-7721.87	-675.44	-654.33	21.11
6	-9520.55	-720.14	-692.42	27.72
7	-11 922.07	-1029.72	-974.78	54.94
8	-14 481.24	-1038.97	-915.62	123.35
9	-16 273.70	-1046.31	-973.51	72.80
10	-18 791.29	-1213.14	-1200.51	12.64
11	-21 113.08	-1054.97	-1025.43	29.54
12	-23 607.39	-1038.59	-987.05	51.54
13	-25 947.96	-1176.65	-1161.15	15.50
14	-28 214.13	-1052.71	-1036.08	16.63
15	-30 727.40	-1124.08	-1109.49	14.59
16	-33 204.14	-1039.82	-991.90	47.92
17	-35 621.82	-1119.26	-1087.09	32.19
18	-38 143.53	-1114.09	-1093.90	20.19
19	-40 726.88	-1103.56	-1093.64	9.92
20	-43 158.11	-1373.04	-1205.35	167.74

levels. We explore several variants on the parallel strategy and greater detail on the exploration of the bare ammonia clusters potential energy surface will be the subject of an upcoming publication where structures for systems as large as  $(\text{NH}_3)_{27}$  will be presented.

The ammonia–hydrogen interaction is significantly smaller than the ammonia–ammonia interaction. As mentioned in Sec. I, we expect the hydrogen molecule to only lightly perturb the structure of the ammonia cluster. Therefore, the strategy we use to explore the minima of the potential energy surface in Eq. (1) is slightly different. Assuming that the presence of one hydrogen molecule would produce only a perturbation on the structure of the minima of the bare system, we search for minima by running trajectories with the hydrogen molecule starting some distance away from a minimum of  $(\text{NH}_3)_{3-20}$  located at the center of the laboratory frame. The structures of  $(\text{NH}_3)_{3-20}$  corresponding to the lowest five energy minima are selected as reasonable starting points. For each ammonia cluster structure, a total of 110 trajectories are started by placing the *para*- $\text{H}_2$  molecule randomly on a sphere of radius  $R_0 = 14.7$  bohrs. For the 5D hydrogen–ammonia surface, the starting orientation of the hydrogen molecule is selected randomly, the center of the hydrogen molecule is placed randomly on a sphere of radius  $R_0 = 16.7$  bohrs, and this process is repeated 110 times as well. For each trajectory, we seek the nearest minimum by using  $T = 0$  Brownian dynamics using the same terminating criteria as for the pure ammonia systems. The lowest minima found for each  $\text{H}_2\text{-(NH}_3)_{3-20}$  are further quenched by tightening the size of the gradient to one part in  $10^8$  to produce the values of  $V_0^d$  in Tables I and II. Additionally, since the global minimum of the ammonia dodecamer and hexadecamer are hollow cages, we start one trajectory for the full 5D surface and one trajectory for the rotationally averaged surface with

TABLE II. Potential energy  $V_0^d$  for the  $H_2-(NH_3)_n$  putative global minimum, the vertical  $H_2$  binding energy  $D_v$ , the  $H_2$  binding energy  $D_e$  with respect to the parent  $(NH_3)_n$ , and the relaxation energy  $\Delta_r$  of  $(NH_3)_n$  from the structure in the optimal  $H_2-(NH_3)_n$  to its closest minimum. Data obtained using the spherically averaged 3D PES for  $H_2-NH_3$ , in  $cm^{-1}$ .

$n$	$V_0^d$	$D_v$	$D_e$	$\Delta_r$
3	-3360.19	-65.76	-65.76	0.00
4	-5485.44	-67.49	-67.49	0.00
5	-7135.94	-68.40	-68.40	0.00
6	-8918.68	-82.91	-82.46	0.45
7	-11 052.36	-90.21	-90.08	0.13
8	-13 645.17	-79.80	-79.56	0.24
9	-15 387.84	-87.70	-87.65	0.06
10	-17 676.80	-86.97	-85.81	1.46
11	-20 176.67	-89.08	-89.02	0.06
12	-22 727.16	-77.40	-77.37	0.03
13	-24 867.42	-80.83	-80.61	0.23
14	-27 263.32	-86.14	-85.26	0.87
15	-29 702.03	-83.61	-84.11	-0.51
16	-32 286.70	-74.84	-74.46	0.38
17	-34 641.14	-109.84	-106.41	3.43
18	-37 156.78	-109.60	-107.15	2.45
19	-39 725.37	-96.98	-92.12	4.86
20	-42 132.42	-93.21	-94.05	-0.86

the hydrogen in their respective centers. In all our minima searches, we allow the degrees of freedom of the ammonia cluster to relax and become distorted by the presence of the hydrogen molecule, and we measure the ammonia–ammonia contribution to the overall potential at the putative global minima for each system. The difference between the latter number and the energy of the global minimum of the bare cluster is the perturbation energy  $\Delta_r$  reported in Tables I and II.

### C. Quantum simulations

In this work, we employed the diffusion Monte Carlo (DMC) method to investigate the most fundamental quantum effects (zero point motion and energy, ZPE) for the title systems. The reason for this choice is twofold. First, zero-temperature simulations appear as the most precise approach to investigate potential transferability as they are expected to be more sensitive to the “wiggles and bumps” of the PES compared to path-integral MC (PIMC) due to the exclusion of the thermal effects. Second, the risk of broken ergodicity while simulating highly quantum object such as  $H_2$  is reduced for DMC compared to PIMC, which would require the use of very long “bead and spring” chains to guarantee convergence for states close to the ground state. Also, the ground state energy  $E_0$ , which is the negative of the adiabatic dissociation energy  $D_0$ , would represent better the relative stability of the different aggregates and the evolution of the former with respect to the ammonia cluster size. Besides,  $E_0$  (or  $D_0$ ) would be the quantity to compare with experimental results on adiabatic desorption processes. Since DMC methods are well described in the literature,<sup>78,79</sup> we provide only the details needed to understand the results presented in the following.

In our simulations,  $H_2$  is treated as a rigid rotor with antisymmetric nuclear spin pairing (i.e., the *para* spin isomer

form) when using the 5D PES, or as a point particle when described by the 3D surface. This choice is due to, first, the orders of magnitude difference between vibrational frequency of the  $H_2$  covalent bond and the rotational constant, and, second, to the possible conversion from *ortho*- $H_2$  to *para*- $H_2$  in presence of a spin center. The sufficiently strong interaction between ammonia and hydrogen molecules allows us to dispense with the use of a guiding wave function, a choice that is expected to reduce the risk of introducing structural biases in the sampled ground state wave function  $\psi_0$ ; thus, the branching step during a DMC simulation is carried out employing the “bare” interaction potential in Eq. (1) as in the original algorithm.<sup>78</sup> We take care, however, in minimizing the “step to step” error during simulations<sup>68</sup> associated with weight truncation, and employed the symmetric  $w = \exp[-\delta t\{V(\mathbf{R}_i) + V(\mathbf{R}_f)\}/2]$  form to define the branching weight of each walker. Here,  $\delta t$  is the time step used in the simulation, whereas  $V(\mathbf{R}_{i,f})$  is the value of the interaction potential of the walker before (*i*) and after (*f*) the diffusion step. The diffusion of the  $H_2$  center of mass is simulated sampling Gaussian distributed displacements with variance  $\delta t/m$ , with  $m = 3672.4$  a.u. being the molecular mass of the hydrogen molecule; the rotational diffusion of  $H_2$  needed in the simulations employing the full 5D ammonia–hydrogen molecules surface is simulated employing a recently proposed algorithm<sup>80</sup> capable of reducing the single step error to second order in the time step  $\delta t$  and third in the curvature  $\mathcal{R}$ . This choice guarantees a robust second order error for the average potential estimator of  $E_0$ , which is employed in this work due to the absence of the trial wave function.

The simulations are all run using a time step  $\delta t = 100$  a.u. and employing 10 000–20 000 walkers to represent the sampled  $\psi_0$  in the attempt of minimizing the population bias associated with the finite size ensemble of replicas. To avoid any possible structural bias due to initial conditions, simulations are started sampling the location of the center of mass of the  $H_2$  molecules randomly inside a cube with side 20–30 bohrs; for the simulations treating explicitly the rotational degrees of freedom of  $H_2$ , the initial orientation of each molecule is chosen sampling a uniform distribution in  $\phi$  and  $\cos \theta$ . Hydrogen molecules with too much overlap with ammonia molecules (creating too much repulsion) are discarded automatically by the DMC simulations when starting the latter with a zero reference energy. To investigate the main characteristics of  $\psi_0$ , we opted for visualizing the CoM distribution of the hydrogen molecule as sampled during the DMC runs. Although more accurate approaches converging to the appropriate limit of sampling  $\psi_0^2$  are available,<sup>81,82</sup> our simple approach has been found useful already in extracting qualitative information for systems that are reasonably strongly bound.<sup>80,83</sup> We will show in the following that this is the case also for the title systems.

## III. RESULTS

### A. Optimization

Tables I and II show the energetic data for the putative global minima obtained as described in Sec. II B. We report

the total potential energy  $V_0^d$  for  $H_2-(NH_3)_n$  species, the vertical dissociation  $D_v$  energy for  $H_2$  (i.e., the difference between  $V_0^d$  and the potential for  $(NH_3)_n$  frozen in the optimal  $H_2-(NH_3)_n$  geometry), the adiabatic dissociation energy  $D_e$  of  $H_2$  with respect to the optimized parent cluster, and the relaxation energy  $\Delta_r$  for the pure ammonia aggregate from the  $H_2-(NH_3)_n$  geometry to the optimal parent ammonia cluster. The reasons that led us to include information on  $D_v$  and  $\Delta_r$  are related to the possibility of a dissociation process (perhaps mediated by photon adsorption) faster than the relaxation of the ammonia aggregates, whose restructuring would have  $\Delta_r$  as driving force.

We begin the discussion on the optimization results by noticing that  $\Delta_r$  is found to be substantially larger when  $H_2$  is treated as a classical rigid body object (rb- $H_2$ , i.e., when described by the 5D PES) than in the case of the spherically averaged potential. We also highlight the 5D relaxation energy for  $n = 8$  and 20 that gives indication of a slightly more marked deformations associated to the “landing” of rb- $H_2$ . The larger values of  $\Delta_r$  from the 5D PES are the direct consequence of its interaction strength (nearly five times stronger than for the 3D PES) in the attractive regions, and its capability of distorting more the underlying ammonia cluster. In the case of the spherically averaged PES, a few  $\Delta_r$  values take a negative signs despite an expected positive value. By restarting trajectories, we were able to confirm that the small negative  $\Delta_r$  for  $n = 15$  and 20 in Table II are indeed related to the optimization threshold; in fact, reducing the maximum size of the gradient led to  $\Delta_r$  values smaller in magnitude.

For both  $D_v$  and  $D_e$ , it appears evident the effect of the spherical average, which eliminates the anisotropy due to the electrostatic quadrupole of  $H_2$  from the  $NH_3-H_2$  interaction. Nevertheless, it is clear from Figure 1 that the  $D_e$  versus  $n$  landscape painted by the two model interactions is fairly similar, with energy differences between neighbor species being scaled downward by the weaker 3D PES.  $n = 14$  and 20 deviates from the mentioned rule as a difference in “curvature” in  $D_e$  (or  $D_v$ ) versus  $n$  is present. A fairer comparison would, however, only be possible using the quantum simulation results, as in the latter case one would also include the quantum

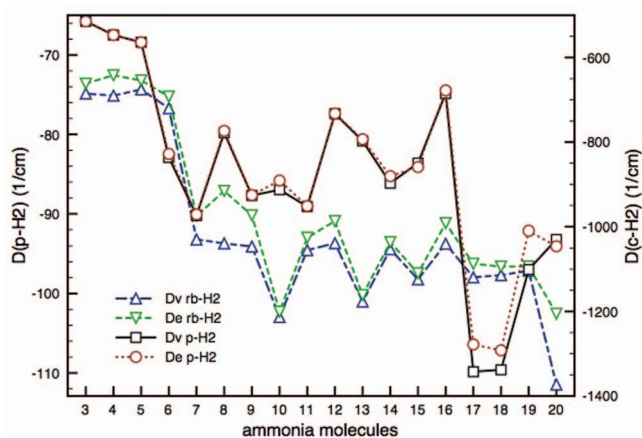


FIG. 1. Vertical and adiabatic dissociation energy ( $D_v$  and  $D_e$ , in  $cm^{-1}$ ) for  $H_2-(NH_3)_n$  as a function of the number  $n$  of ammonia molecules. The left axis refers to species containing *para*- $H_2$ , while the right axis refers to species containing the rigid-body  $H_2$  described by the 5D PES.

rotational motion of rb- $H_2$ . Since doing so allows one to understand better the interplay between rotational averaging and vibrational motion, we shall discuss DMC results with this point of view in mind (*vide infra* Sec. III B).

As for the relative fluctuation of the binding energy versus  $n$ , we notice that these are spread over a range of roughly 30% of the largest  $D_e$  in magnitude for both PESs when  $n \geq 7$ . Thus, no major size effects appear in this range. The binding energy is, instead, substantially lower when  $n < 7$ . It is also worth highlighting and bearing in mind the cases of *para*- $H_2-(NH_3)_{17}$  and *para*- $H_2-(NH_3)_{18}$ , for which the large magnitude of  $D_e$  may indicate possible surface peculiarities. To investigate the root causes for the mentioned finding, Figures 2–5 show the structure of the putative global minima for  $H_2-(NH_3)_n$  ( $n = 3-20$ ).

From these, we notice that the lower magnitude of  $D_e$  for  $n < 7$  is related to a different location of  $H_2$  than in the larger systems. In fact, both PESs collocate  $H_2$  externally on the plane of the ring when  $n = 3-5$ , and over a tetrameric ring of the “book” form<sup>64</sup> for  $n = 6$ . Albeit small differences are present in term of the precise location between the two PESs,

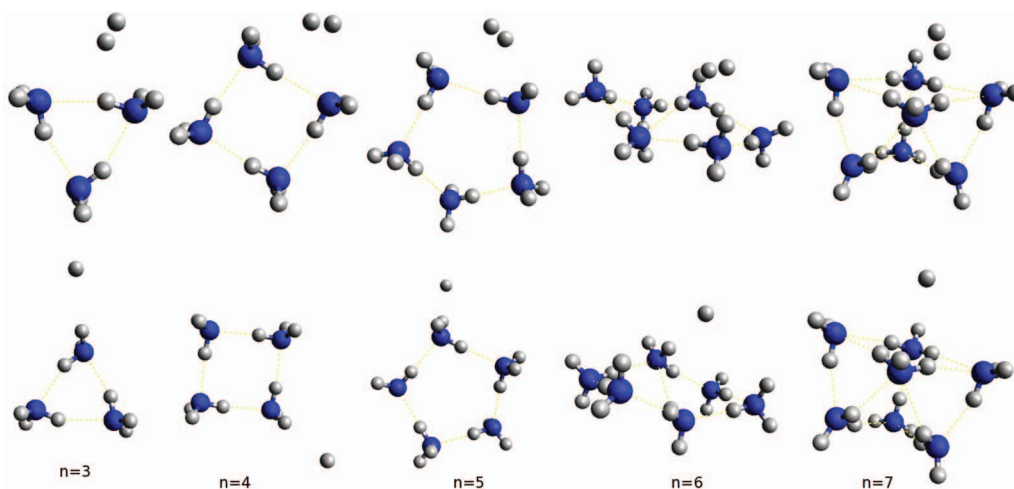


FIG. 2. Putative global minimum structure for  $H_2-(NH_3)_n$  ( $n = 3-7$ ). (Top row) rb- $H_2$  described by the 5D PES; (bottom row) *para*- $H_2$ .

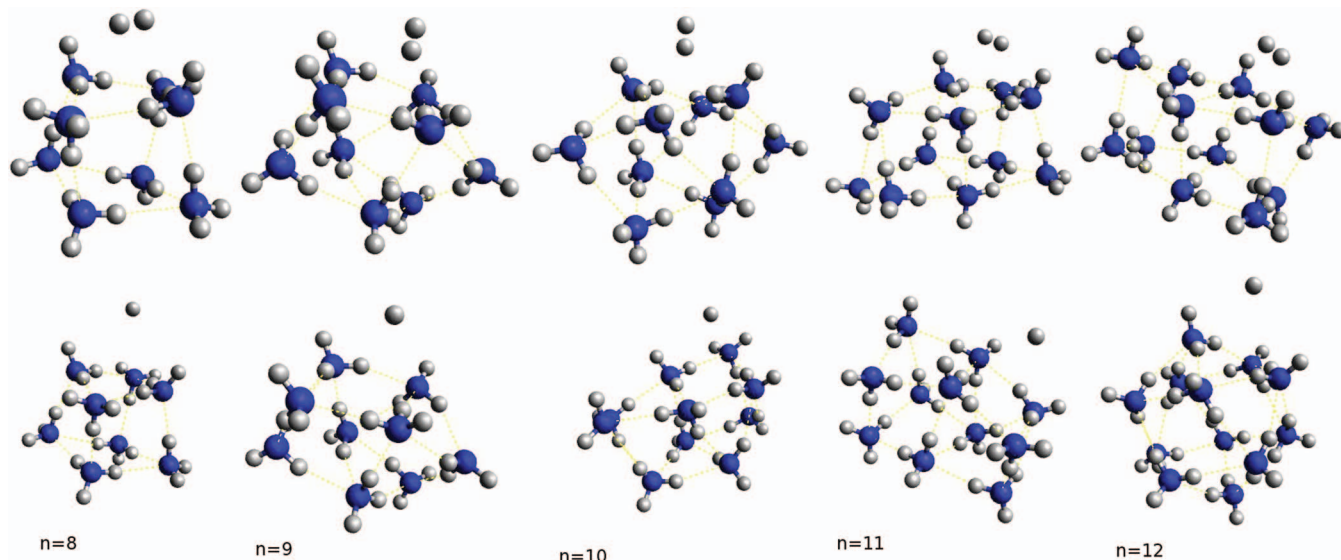


FIG. 3. Putative global minimum structure for  $\text{H}_2-(\text{NH}_3)_n$  ( $n = 8-12$ ). (Top row)  $\text{rb-H}_2$  described by the 5D PES; (bottom row)  $\text{para-H}_2$ .

there is an overall agreement between the main features (also, *vide infra* for DMC simulations).

For the  $\text{para-H}_2-(\text{NH}_3)_n$  species with  $n \geq 7$ , the putative global minima are mainly characterized by a surface binding motif built by rhomboidal ammonia tetramers (henceforth “rhombus”) containing two double donor (DD) and two double acceptor (AA) molecules (e.g., see the topmost face of  $\text{H}_2-(\text{NH}_3)_8$ ). Notice that with this spatial disposition, the DD ammonia molecules interact with  $\text{para-H}_2$  via PES minimum along the  $C_3$  axis on the molecular H-side ( $D_e = -28.3 \text{ cm}^{-1}$ ); the two AA molecules, instead, interact via the N-side minimum ( $D_e = -23.7 \text{ cm}^{-1}$ ). Deviations from this common motif are found for  $n = 13, 14$ , and  $17-20$ . In the case of  $n = 13$ , there is an open ring as a result of one of the DD molecules being connected with an ammonia sitting in a layer underneath the one of the rhombus interacting

with  $\text{H}_2$ ; aside from this detail, the overall structure is maintained.  $\text{H}_2-(\text{NH}_3)_{14}$ , instead, has a different H-bond topology, containing two donor-acceptor (DA) molecules as part of the tetrameric ring together with a DD and an AA molecule. The differences in the larger clusters emerge from the more complicated surface structure, which features adsorbed molecules with unsaturated H-bond that can be donated directly to  $\text{H}_2$  without competing with other molecules. This is particularly evident for  $N = 17$  in Figure 4; retrospectively, such finding rationalizes the higher binding energy for the larger species seen in Figure 1. Similarly, the nearly constant  $D_b$  for species with  $N = 8-16$  is well supported by the common  $\text{H}_2$  binding motif, with deviation being correlated mainly to differences in the distances and angles of the surface tetramer.

Similar conclusions emerge for the case of  $\text{rb-H}_2-(\text{NH}_3)_n$  ( $n = 8-20$ ). In other words, the binding location

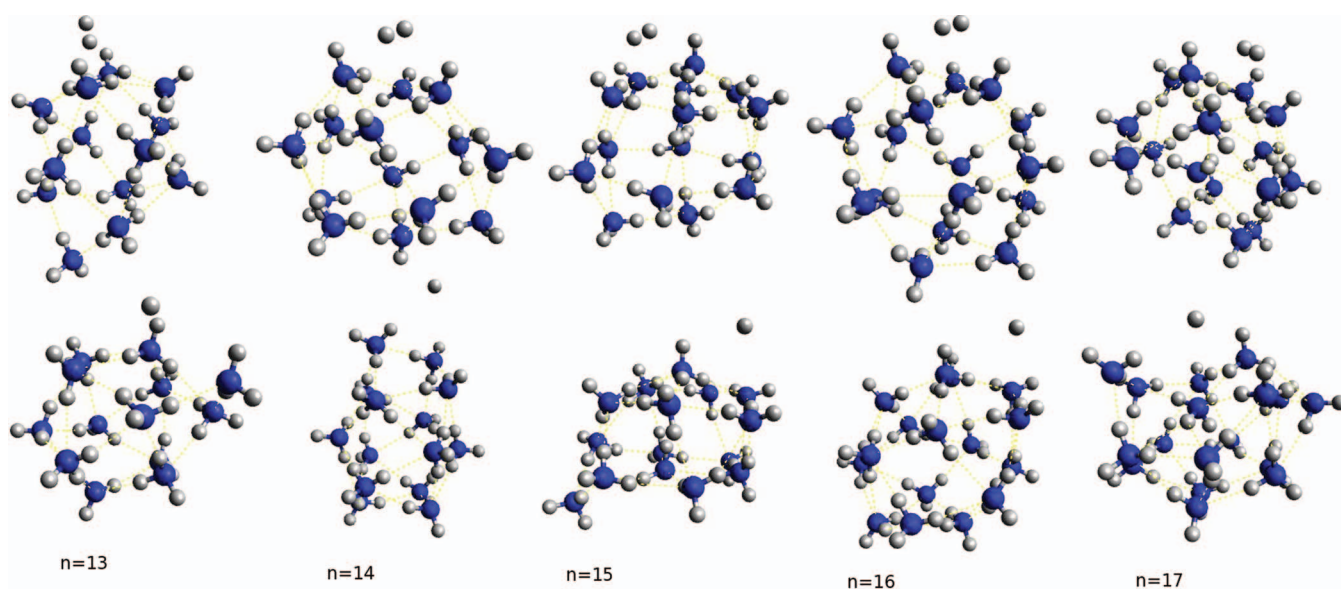


FIG. 4. Putative global minimum structure for  $\text{H}_2-(\text{NH}_3)_n$  ( $n = 13-17$ ). (Top row)  $\text{rb-H}_2$  described by the 5D PES; (bottom row)  $\text{para-H}_2$ .

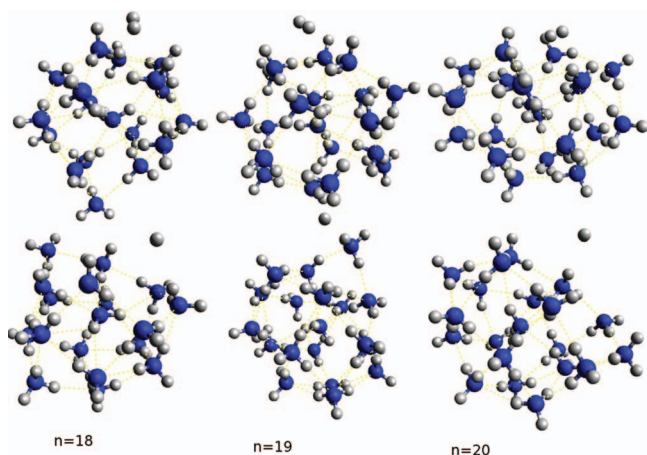


FIG. 5. Putative global minimum structure for  $\text{H}_2\text{-(NH}_3)_n$  ( $n = 18\text{--}20$ ). (Top row)  $\text{rb-H}_2$  described by the 5D PES; (bottom row)  $\text{para-H}_2$ .

presents always an interaction between  $\text{rb-H}_2$  with the aforementioned rhomboidal ring. Even in this case, the oscillations in  $D_e$  and  $D_v$  versus  $n$  are to be attributed to differences in the local structure of the tetrameric ring and, consequently, to the final orientation of  $\text{rb-H}_2$ . In many of the cases shown in Figures 2–5, the dominant interaction mode seems to be the one related to the deepest minimum of the  $\text{rb-H}_2\text{-(NH}_3)_n$  potential,<sup>63</sup> with  $\text{rb-H}_2$  donating a hydrogen bond to the lone pair side of vicinal ammonia molecules. The only deviation from a “rhombus” landing site is represented by the presence of an ad-ammonia absorbed nearby in  $(\text{NH}_3)_{20}$  (see the top face of  $\text{H}_2\text{-(NH}_3)_{20}$  in Figure 5). Such feature represents an additional source of interaction for the rigid-body  $\text{H}_2$ , which can thus increase its binding energy with the ammonia cluster. It is such additional stabilization that rationalizes the larger magnitude of the vertical binding energy seen for  $n = 20$  in Figure 1.

## B. DMC simulations

From the species obtained using the optimization stage described in Sec. III A, we selected a few systems for further investigation by means of the DMC method. The criteria for the selection were based on the opportunities to better comprehend the competition between the most attractive structural motif (rhombus-like) present in the globally optimized species, and the most likely ones (trimeric and tetrameric rings) emerging from the simulation of ultra-cold cluster formation.<sup>60</sup> As indicated above, the vast majorities of the putative global minima are derived from the adsorption of  $\text{H}_2$  on the cluster surface in correspondence with a closed rhomboidal disposition of two AA and two DD ammonia molecules and without any substantial rearrangement in  $(\text{NH}_3)_n$ . Thus, our DMC simulations employed the global minimum structure for the parent ammonia clusters keeping the latter frozen. The rationale behind this choice is related to the strong binding energy in ammonia clusters, the high interconversion barriers between their isomers,<sup>70</sup> and the structural stability indicated by DMC calculations for pure clusters other than the pentamer.<sup>71</sup> This choice, obviously, also

TABLE III. DMC  $E_0$  ( $=-D_0$ ),  $D_e$  binding energy (from Table I) and anharmonic ZPE for  $\text{rb-H}_2\text{-(NH}_3)_n$  with the hydrogen molecule described using the full 5D PES. Data in  $\text{cm}^{-1}$ ; the standard error of the data is smaller than the last digit shown.

$n$	$E_0$	$D_e$	ZPE
3	−13.61	−661.68	648.07
4	−8.52	−641.95	636.43
9	−40.14	−1046.31	1006.16
12 <sup>a</sup>	−22.25	−1038.59	1016.33
12 <sup>b</sup>	−31.40	−1010.44	979.03
16	−26.05	−1039.82	1013.77
17	−28.37	−1119.28	1090.90

<sup>a</sup> $(\text{NH}_3)_{12}$  with the same structure found for the global minimum of  $\text{H}_2\text{-(NH}_3)_{12}$ .

<sup>b</sup> $(\text{NH}_3)_{12}$  with the same structure found for the global minimum of pure  $(\text{NH}_3)_{12}$ .

excludes possible effects due to the couplings (if any, given the difference in energy<sup>84,85</sup>) between intramolecular ammonia modes and  $\text{H}_2$  quantum motion.

Since the ammonia moiety in the global minimum for  $\text{rb-H}_2\text{-(NH}_3)_{12}$  differs from the global minimum of  $(\text{NH}_3)_{12}$ , we deviated from the above prescription and employed both ammonia skeletons. For comparative purposes, a similar strategy is also applied to  $\text{para-H}_2\text{-(NH}_3)_{12}$ , simulating  $\psi_0$  of both the first and second lowest minima obtained using the 3D PES. We notice that the second lowest minimum for the latter surface is structurally equivalent to the global minimum of the full 5D one; in other words, there is an inversion of the relative structural stability, albeit the potential energy difference is only  $\sim 70 \text{ cm}^{-1}$ .

In the simulation set, we also included the ammonia heptadecamer as it has an ammonia molecule sitting on the surface of the clusters with unsaturated N–H group close to a rhombus. Our optimization employing the 3D PES suggested the latter to be the preferential adsorption site. Finally, we also included  $\text{H}_2\text{-(NH}_3)_3$  and  $\text{H}_2\text{-(NH}_3)_4$  for the sake of completeness, employing the cyclic global minima as they are often present in species formed in ultra-cold conditions.<sup>60</sup>

Tables III and IV show the results obtained with the DMC simulations, together with the dissociation energy  $D_e$  defined before (see Sec. III A). We begin by indicating that the spherically averaged PES appears perfectly able to reproduce the

TABLE IV. DMC  $E_0$  ( $=-D_0$ ),  $D_e$  binding energy (from Table II) and anharmonic ZPE for  $\text{H}_2\text{-(NH}_3)_n$  with the hydrogen molecule described as a spherical object using the rotationally averaged PES for  $\text{para-H}_2$ . Data in  $\text{cm}^{-1}$ ; the standard error of the data is smaller than the last digit shown.

$n$	$E_0$	$D_e$	ZPE
3	−8.70	−65.76	57.06
4	−5.98	−67.49	61.51
9	−29.27	−87.70	58.43
12 <sup>a</sup>	−24.15	−77.40	53.25
12 <sup>b</sup>	−15.69	−76.79	61.10
16	−18.34	−74.84	56.50
17	−20.96	−109.84	88.88

<sup>a</sup> $(\text{NH}_3)_{12}$  with the same structure found for the global minimum of  $\text{para-H}_2\text{-(NH}_3)_{12}$  and  $(\text{NH}_3)_{12}$ .

<sup>b</sup> $(\text{NH}_3)_{12}$  with the same structure in the second lowest minimum of  $\text{para-H}_2\text{-(NH}_3)_{12}$ , which is similar to the global minimum for  $\text{H}_2\text{-(NH}_3)_{12}$ .



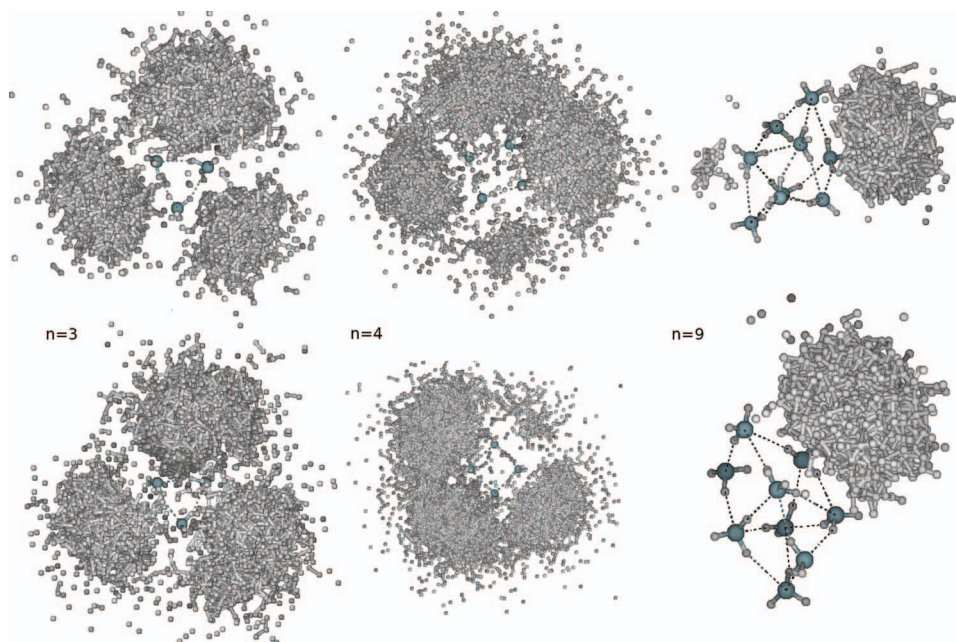


FIG. 6. Graphical representation of the  $\text{H}_2$  center of mass distribution obtained from  $\psi_0$  as sampled by DMC for  $\text{H}_2-(\text{NH}_3)_n$  ( $n = 3, 4,$  and  $9$ ). (Top row)  $\text{para-H}_2$  described by the 5D PES; (bottom row)  $\text{para-H}_2$ .

relative energy ordering (hence, the hydrogen binding energy) suggested by the more complicated 5D PES. In other words, the relative stability of the clusters studied is the same despite the substantial simplification introduced by the spherical averaging. We also note that  $E_0$  results produced using the 5D PES are always larger in magnitude (i.e.,  $\text{H}_2$  is more strongly bound) than for the spherically averaged 3D potential. This finding is indeed not surprising in light of the possibility afforded by the rigid rotor  $\text{H}_2$  to better adapt its wave function to the wiggles and bumps of the surface potential generated by the underlying ammonia clusters. The difference between  $E_0$  obtained employing the two PESs are in the range  $7\text{--}11\text{ cm}^{-1}$  for the larger clusters, with the tendency of presenting larger differences for the more strongly bound  $\text{H}_2$ . Clearly, a more precise match between quantum binding energies from the two PESs would represent a valuable result. Two facts must however be considered while drawing a conclusion: first, the 5D potential energy landscape for  $\text{H}_2$  is quite rough and the rigid rotor model is better able to adapt to the surface; second, even the adiabatic treatment of  $\text{H}_2$  rotation in the simpler  $\text{H}_2\text{--H}_2\text{O}$  complex indicates important effects due to hindered rotations.<sup>65</sup> In view of these observations and since the relative difference in  $E_0$  between the 3D and 5D sets of DMC results is at most 1% of the ZPE for the 5D PES, it is not unreasonable to consider the 3D PES as providing an overall sound description of the  $\text{para-H}_2/\text{NH}_3$  interaction.

A closer look at the relative  $D_e$  and  $E_0$  stability as a function of  $n$  highlights the fact that these do not run parallel to each other. For instance, we notice that the relative ordering for the dodecamer described with the 5D PES is inverted, and that the nonamer becomes fairly more stable than the heptadecamer when simulated with DMC. Similar inversions are also found for the 3D PES, albeit the initial difference in  $D_e$  are clearly reduced by the spherically averaged surface. We interpret the presence of such energetic reordering as directly

connected to the quantum nature of the adsorbed species, for which an increased localization due to a somewhat deeper (and likely also narrower) well of the global minimum may induce a higher kinetic energy content in the system.<sup>71,83,86</sup> To explore such possibility, we visually investigate the distribution of the center of mass for the hydrogen molecule as sampled by means of DMC simulations employing both interaction surfaces. Figures 6 and 7 show a few snapshots collected from walker populations of roughly 10 000 replicas.

The result for the small clusters are presented in Figure 6, and they show that similar distributions are built by the two surfaces. Thus, the small structural differences between the two PESs shown in Figure 2 for  $n = 3$  and  $4$  are “smeared out” by the quantum motion. In fact, both  $\text{H}_2-(\text{NH}_3)_3$  and  $\text{H}_2-(\text{NH}_3)_4$  show the center of mass of both rigid-body and  $\text{para-H}_2$  to be distributed externally to the clusters and reproducing fairly well the axial symmetry of these species. For  $\text{H}_2-(\text{NH}_3)_9$ , we notice that the highest population is found above the rhombus that provides the strongest interaction with  $\text{H}_2$  (i.e., the one on which the hydrogen molecule is adsorbed to form the lowest minimum), albeit for the rigid-body hydrogen molecule there is secondary lobe located over another rhomboidal structure opposite to the lowest potential adsorption site. Interestingly, the latter structure has the two opposite DD molecules presenting their dangling N–H bond closer in orientation to the vector normal to the average plane defined by the four N atoms than the case of the lowest potential adsorption site. Such structural detail seems to disfavor the buildup of a local density of adsorbed  $\text{H}_2$  for both PES, albeit it does that more for the 3D potential than for the 5D one. The latter may exploit the additional degrees of freedom to better adapt its distribution in order to interact more attractively with the potential surface, as suggested above.

Figure 7 displays the hydrogen distribution for the remaining clusters simulated with DMC. The main theme

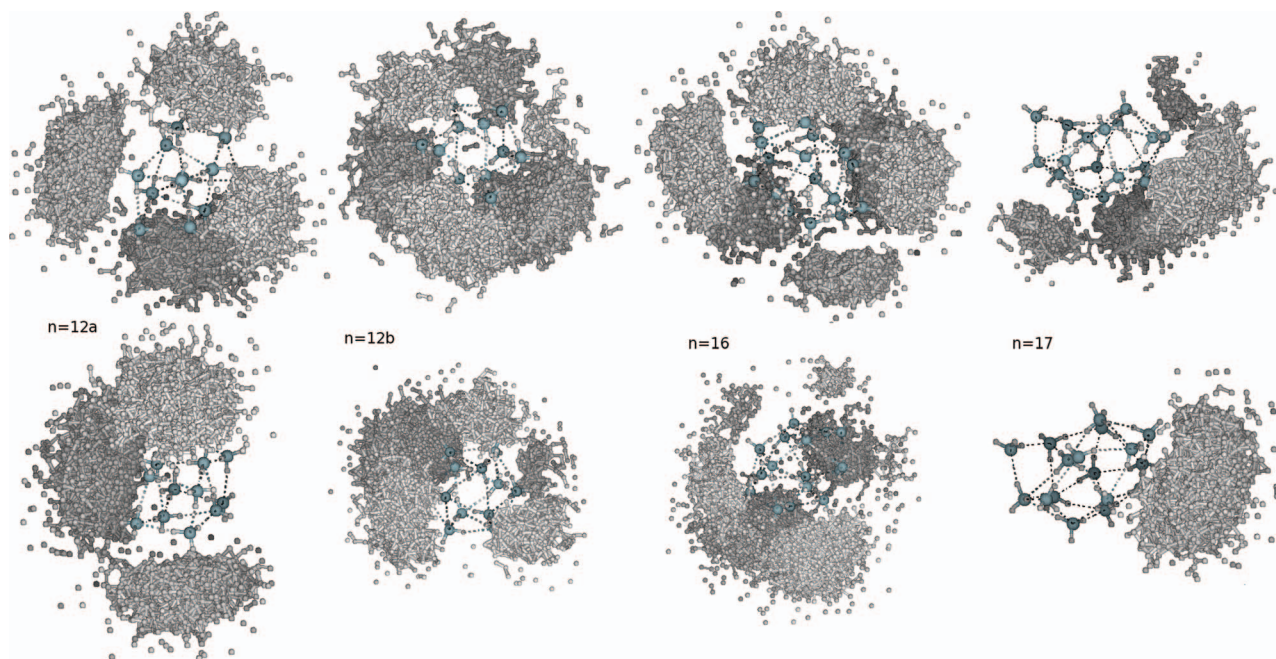


FIG. 7. Graphical representation of the  $H_2$  center of mass distribution obtained from  $\psi_0$  as sampled by DMC for  $H_2-(NH_3)_n$  ( $n = 12, 16$ , and  $17$ ). The label 12a refers to the simulations run using the ammonia skeleton that gives the lowest minimum for  $n = 12$  while using the 5D PES (distorted bicubic structure), while 12b indicates simulations run using the lowest minimum of the pure ammonia cluster. (Top row)  $rb-H_2$  described by the 5D PES; (bottom row)  $para-H_2$ .

emerging from the pictures appears to be, again, the localization of the density above the rhombus motifs on the surface, with a complete disregard for the structural motifs that are more likely to appear under ultra-cold formation conditions.<sup>60</sup> The asymmetries present in the distribution for  $n = 12$  and  $16$  are justified by both the presence of slight structural differences and by the fact that DMC is expected to be able to produce a perfectly balanced coverage *only* in the limit of an infinite number of replicas. It is only in this case that the population bias introduced by the population control<sup>87</sup> and by non-completeness of the basis set used vanishes.<sup>68</sup> In presence of large energy barriers separating the attractive regions of the potential, one should thus not be surprised by an unbalanced distribution as we indeed obtained; the latter, however, still presents a population over all energetically similar minima.

In the case of  $(NH_3)_{12}$  highlighted above due to the inversion of stability between the two isomers, we notice that the global minimum of  $rb-H_2-(NH_3)_{12}$  contains only four rhombuses, each separated from the other three by a tetrameric ring motif as in Figure 6. The global minimum for the reduced PES, instead, presents six rhombuses sharing all vertex ammonia molecules, together with eight trimer rings. Overall, the second species is characterized by a higher curvature of its surface, which has the net effect of affording a larger volume over each rhombus before  $H_2$  is forced to overlap with a less binding (or repulsive) region above a cyclic trimer motif. The lower curvature of the global minimum  $rb-H_2-(NH_3)_{12}$  has also, and perhaps more importantly, the net effect of forcing the dangling N-H bonds of the two AA ammonia molecules in the skeleton to be more perpendicular with respect to the rhombus plane than in the case of the dodecahedral moiety; the same happens for the two competing rhombuses in the nonamer (*vide supra*).

Extending the same analysis to the other systems, it emerges that there is a striking correlation between the relative stability, defined by  $E_0$  in Tables III and IV, and the width of the rhomboidal well over which the highest  $H_2$  density dwells (see Figures 6 and 7). The width is gauged using the distance between the H atoms in the upward pointing dangling N-H bonds of the two AA molecules. Direct inspection of the cluster structures, in fact, gives 5.09, 4.91, 4.75, 4.46, and 4.39 Å, respectively, for the most and least populated rhombuses in  $H_2-(NH_3)_9$ , the most symmetric dodecamer, the heptadecamer, and both the hexadecamer and the least symmetric dodecamer. Such ordering clearly runs parallel to the relative stability ranking obtained by DMC for both PESs, the difference in energetic position between the hexadecamer and the least symmetric dodecamer being defined by subtler effects such as the fact that the rhombus on the hexadecamer is surrounded only by trimer rings. According to our energy data, these afford an improved stability to the adsorbed species compared to the tetrameric rings surrounding the adsorption site in the dodecamer.

Turning to the case of the heptadecamer, it is striking that the global minimum region for the 3D PES is indeed not populated *at all* despite its  $22\text{ cm}^{-1}$  lower classical  $D_e$  than for the nonamer; the whole population of replica is in fact displaced onto the surface rhombus interacting with  $H_2$  in the global minimum of the 5D PES. Inspecting the rhombus underlying the global minimum for the reduced PES indeed provides a justification for the DMC results, as the hydrogen atoms of the two AA dangling N-H bonds sit at 4.20 Å from each other, a distance that is clearly shorter than the one in the populated rhombus in  $(NH_3)_{17}$  and, for what it matters, any other populated rhombus among the investigated clusters. In our eyes, this is a staggering indication that the stronger confinement

required to *para*-H<sub>2</sub> in order to populate the surface region of the global potential minimum plays indeed the key role, inducing a quantum spill-over into surface regions with more relaxed or absent geometrical restraints.

### C. Clathrate-like species: H<sub>2</sub>@(NH<sub>3</sub>)<sub>12</sub> and H<sub>2</sub>@(NH<sub>3</sub>)<sub>16</sub>

One of the long term reasons for developing a H<sub>2</sub>/NH<sub>3</sub> PES and using it in quantum simulations of H<sub>2</sub>-NH<sub>3</sub> mixtures is to foster a better understanding of their thermodynamics and phase diagram with a view toward fuel storage. Therefore, we decided to investigate the energetics of species whose water counterparts may play a role in developing hydrogen storage technology. Recognizing that the global minima of (NH<sub>3</sub>)<sub>12</sub> and (NH<sub>3</sub>)<sub>16</sub> are hollow cages, we thus run DMC simulations with H<sub>2</sub> placed inside these clusters in a clathrate-like configuration. Our initial unbiased search for potential energy minima showed no indication for these species among the stationary structures obtained. Therefore, one might be led to conclude that confining the hydrogen molecule may be energetically expensive compared to the surface adsorption. Indeed, a local optimization starting from the preformed ammonia dodecamer and hexadecamer gave a binding energy, respectively, of +351(+702) and +65(+330) cm<sup>-1</sup> for the 5D(3D) PES. By itself, this conclusion is already non-trivial, as the internal width of the cages and the features of both the 5D and 3D PESs would, at least in principle, allow a stabilizing superposition of attractive regions of the H<sub>2</sub>-NH<sub>3</sub> PES. Notice that the volume inside (NH<sub>3</sub>)<sub>12</sub> and (NH<sub>3</sub>)<sub>16</sub> is smaller than the one inside the water dodecahedron found in clathrate hydrates,<sup>39</sup> where an overall attractive region for a single H<sub>2</sub> is found.<sup>37,38</sup> It must, however, be recalled that such accommodating structure is created at the expenses of a substantial amount of work ( $P \sim 200$  MPa,  $T = 249$  K) employed to restructure the spatial distribution of water molecules.<sup>36</sup>

Congruently with the classical data, our DMC results indicate that H<sub>2</sub> is not stable inside the two cages investigated. For the 5D PES, we found  $E_0 = 1097.2(3)$  and  $658.1(4)$  cm<sup>-1</sup> for the dodecamer and the hexadecamer, respectively. The 3D PES, instead, gave  $E_0 = 1123.6(1)$  and  $698.9(1)$  cm<sup>-1</sup>. Comparing the two sets of results, we observe good correspondence between the two models in terms of the energetic ordering they predict. In terms of the ZPE of the engulfed molecules, the ammonia cages represent indeed much stronger confining regions than the water clathrates previously studied,<sup>37,38</sup> for which it is found that  $ZPE = 177.2$  cm<sup>-1</sup> and that it is possible to include two molecules while still having  $E_0 < 0$ .

With respect to the possible fate of the two clathrate-like species under discussion, we notice that they resemble a particle (H<sub>2</sub>) inside a nearly spherical well, which has  $E_0 \propto 1/R^2$ , with  $R$  being the average radius. Thus, H<sub>2</sub> inside the cages is akin to a gas that exerts a pressure  $p$  onto the internal surface of a container of volume  $V \propto R^3$ , as  $-k_B T (\frac{\partial \ln Z}{\partial V})_T$  (the statistical mechanics definition of pressure) is non-zero even at  $T = 0$  K. The mechanical energy  $pV$  stored in the system may, in principle, lead to a cage expansion, possibly its breakup or, more likely, a restructuring of its hydrogen bond

network. The maximum amount of mechanical energy stored in the system available for carrying out work would, however, be  $E_0$  (the difference between the ground state energy of the caged and un-caged H<sub>2</sub>), which is at most 1.9 kcal/mol. As breaking a single hydrogen bond in ammonia clusters is expected to require more than 4 kcal/mol, it appears that the caged species ought to be considered metastable as they do not contain sufficient energy for breaking up. In other words, such species may be kinetically stable and able to survive at low temperature if formed, thus behaving in a way similar to the hydrogen clathrates. The latter remain stable upon decreasing the pressure to 100 KPa from the 200 MPa needed for the synthesis provided  $T$  remains below 248 K. Clearly, a more definitive conclusion should be sought by simulating the quantum ground and low temperature states of our clathrate-like species employing either DMC or a curved manifolds version of the ring polymer dynamics.<sup>88</sup>

## IV. DISCUSSION AND CONCLUSIONS

Guided by general and specific interests in describing molecules weakly interacting with solid surfaces, we have explored the classical and quantum energy landscape of the H<sub>2</sub>-(NH<sub>3</sub>) <sub>$n$</sub>  systems,  $n = 3-20$ . Employing both 5D and rotationally averaged 3D PESs to locate putative global minima for the mentioned systems, we found that the two PESs provide similar energy landscapes with H<sub>2</sub> physisorbed on the clusters, and that the most common adsorption site has a rhomboidal disposition of the N atoms belonging to two AA and two DD ammonia molecules. Albeit usually topologically connected by hydrogen bonds, the DD molecules donate a hydrogen bond to a NH<sub>3</sub> outside the rhomboidal structure in a few cases. The preferential orientation of *rb*-H<sub>2</sub> with respect to the rhomboidal plane is found to be guided by the donation of a hydrogen bond to a nitrogen. No marked changes in structure are found for the ammonia moiety in H<sub>2</sub>-(NH<sub>3</sub>) <sub>$n$</sub>  compared to pure clusters.

Similar adsorption sites are found for both *rb*-H<sub>2</sub> and *para*-H<sub>2</sub> when simulated using DMC, the correlation of  $D_0$  with the width of the hydrogen rim in each rhombus indicating the key role played by confining forces. Frequently, the H<sub>2</sub> density is located onto the classical minimum adsorption site; only occasionally it also dwells over rhombuses with higher potential energy, but with lower density (see  $n = 9$  and 17). However, neither *rb*-H<sub>2</sub> nor *para*-H<sub>2</sub> are ever found with density on rhombuses with a surface adsorbed NH<sub>3</sub> nearby, and this is despite the fact that these sites are the most strongly bound from the classical potential point of view. Notice that the strong correlation between  $E_0$  (or  $D_0$ ) and the width of the hydrogen rim over the rhombuses, together with the lack of H<sub>2</sub> population on top of square and triangular motifs allow one to predict the H<sub>2</sub> adsorption energy on the surfaces of larger aggregates as ammonia ices. It would be, in fact, sufficient to measure the distance between the dangling H atoms of the DD molecules in a rhombus to obtain an estimate for  $E_0$  from our data.

Finally, clathrate-like species (i.e., the hollow (NH<sub>3</sub>)<sub>12</sub> and (NH<sub>3</sub>)<sub>16</sub> filled with a single H<sub>2</sub>) are not stable when compared to the parent clusters plus hydrogen molecule.

However, the “quantum pressure” exerted by the engulfed H<sub>2</sub> does not seem to be sufficiently strong to force a hydrogen-bond breaking and its consequent escape. This conclusion, however, needs to be carefully tested against simulations describing the ammonia skeleton as fully flexible, which ought to involve additional development for DMC or the curved manifolds version of the ring polymer dynamics.<sup>88</sup> Work along these directions is in progress in our laboratories.

The direct comparison of the 5D and 3D PESs data highlights an overall good capability of the reduced potential in providing qualitatively (in terms of the location) and semi-quantitatively (maximum error in E<sub>0</sub> of ~1% of the ZPE generated by using the 5D PES) correct results. The discrepancy between the two models is mainly due to the absent ability of *para*-H<sub>2</sub> to adapt to the local surface “nuances.” Worth mentioning is the finding that *rb*-H<sub>2</sub> remains hydrogen bonded to the nitrogen of NH<sub>3</sub> during DMC simulations; *para*-H<sub>2</sub> prefers instead the region along the C<sub>3</sub> axis on the H-side (results not shown). Comparing the latter results indicates that *rb*-H<sub>2</sub> may behave as a very anharmonic pendulum.

To contextualise our work, it is useful to compare with the case of H<sub>2</sub> adsorbed on water ice. We begin noticing that our global minima involving *rb*-H<sub>2</sub> have a larger D<sub>e</sub> than found for a model of rigid amorphous ice (deviations in the range 75–310 cm<sup>-1</sup>).<sup>1</sup> This is due to a deeper well in our ammonia–H<sub>2</sub> surface compared to the water–H<sub>2</sub> model,<sup>89</sup> the latter being too weakly binding compared to more recent surfaces.<sup>90</sup> Besides, the amorphous ice has a rougher surface than our molecular-size grains. Despite the relative interaction strengths and the surface disorder, our DMC results provide smaller D<sub>0</sub> than obtained simulating H<sub>2</sub> on the amorphous ice (175–640 cm<sup>-1</sup>).<sup>2</sup> As it seems that H<sub>2</sub> adsorbs onto the ice in location structurally similar to the ones on our clusters, and that the E<sub>0</sub> = –20.98 cm<sup>-1</sup> for H<sub>2</sub>–NH<sub>3</sub> obtained with the 5D PES compares well with E<sub>0</sub> = –34.74 cm<sup>-1</sup> for H<sub>2</sub>–H<sub>2</sub>O computed using a PES with a well of D<sub>e</sub> = –234.15 cm<sup>-1</sup>,<sup>90</sup> we find the discrepancy in D<sub>0</sub> somewhat puzzling and difficult to reconcile. Unfortunately, no direct comparison with experimental results is possible, as the approach used for modeling empirical H<sub>2</sub> desorption data from water ice implies a complicated ensemble average.<sup>7</sup> As possible explanation, we suggest that the amorphous ice surface might be rich on under-coordinated O atoms, which would represent a preferential H<sub>2</sub> adsorption site<sup>2</sup> due to the stronger interaction. An equivalent situation, with surface N atoms exposing their uncumbered side outward, is not present in our systems.

Turning to the H<sub>2</sub> tagging employed to improve spectroscopic resolution, we notice that our quantum binding energies (–40/–22 cm<sup>-1</sup>, or –62/–34 K) support the possibility of adding H<sub>2</sub> to a pre-formed ammonia cluster inside a He droplet. It should also be possible to tag clusters in molecular beams studies, albeit aggregates may need to be sufficiently cold. Importantly, our data indicate a marked preference for the rhomboidal motif, which is seldom found when a fast energy dissipation is expected.<sup>60</sup> Nevertheless, the most frequent (and least bound, see Tables III and IV) tetrameric motif<sup>60</sup> should bind H<sub>2</sub> strongly enough to generate a stable adduct. A competition for H<sub>2</sub> between this motif and trimeric rings, also present in clusters formed under strong dissipation

regime,<sup>60</sup> should however be expected based on the relative stability and frequency. Such peculiarity may be exploited to shed some light on the ammonia clusters formed by seeding He droplets by recording the rotational spectrum of the adsorbed H<sub>2</sub>.<sup>3</sup>

We would like to conclude recalling that the thrust for developing a H<sub>2</sub>–NH<sub>3</sub> PES is the study of their condensed phase aggregates, hoping to find phases or conditions useful in fuel storage technology. In this respect, it seems fair to compare the interaction strength of the 5D PES with possible storage materials as aromatic frameworks.<sup>91</sup> We thus notice that correlated calculation on a few aromatic species<sup>92</sup> place the D<sub>e</sub> of H<sub>2</sub> in the 290–350 cm<sup>-1</sup> range, which is lower than for the 5D PES (see Table I). Thus, it may seem that pores in amorphous ammonia ice might be capable of binding more strongly a few hydrogen molecules than graphene nanostructures,<sup>91</sup> zeolite imidazolate frameworks,<sup>93</sup> but not carbon foams.<sup>94</sup>

## ACKNOWLEDGMENTS

E.C. acknowledges the donors of the Petroleum Research Fund, administered by the ACS (Grant No. 48146-B6), The Stacy Ann Vitetta ’82 Professorship Fund, and The Ellington Beavers Fund for Intellectual Inquiry from Arcadia University for support of this research. M.M. acknowledges funding from the Università dell’Insubria under the scheme “Fondi di Ateneo per la Ricerca di Base.”

- <sup>1</sup>H. G. Hixson, M. J. Wojcik, M. S. Devlin, J. P. Devlin, and V. Buch, *J. Chem. Phys.* **97**, 753 (1992).
- <sup>2</sup>V. Buch and J. P. Devlin, *J. Chem. Phys.* **98**, 4195 (1993).
- <sup>3</sup>V. Buch, S. C. Silva, and J. P. Devlin, *J. Chem. Phys.* **99**, 2265 (1993).
- <sup>4</sup>H. B. Perets, O. Biham, G. Manicó, V. Pirronello, J. Roser, S. Swords, and G. Vidali, *Astrophys. J.* **627**, 850 (2005).
- <sup>5</sup>F. Dulieu, L. Amiaud, S. Baouche, A. Momeni, J.-H. Fillion, and J. Lemaire, *Chem. Phys. Lett.* **404**, 187 (2005).
- <sup>6</sup>L. Hornekaer, A. Baurichter, V. V. Petrunin, A. C. Luntz, B. D. Kay, and A. Al-Halabi, *J. Chem. Phys.* **122**, 124701 (2005).
- <sup>7</sup>L. Amiaud, J. H. Fillion, S. Baouche, F. Dulieu, A. Momeni, and J. L. Lemaire, *J. Chem. Phys.* **124**, 094702 (2006).
- <sup>8</sup>J.-H. Fillion, L. Amiaud, E. Congiu, F. Dulieu, A. Momeni, and J.-L. Lemaire, *Phys. Chem. Chem. Phys.* **11**, 4396 (2009).
- <sup>9</sup>V. Buch, J. Sadlej, N. Aytemiz-Uras, and J. P. Devlin, *J. Phys. Chem. A* **106**, 9374 (2002).
- <sup>10</sup>J. P. Devlin, D. B. Gulluru, and V. Buch, *J. Phys. Chem. B* **109**, 3392 (2005).
- <sup>11</sup>P. Ayotte, P. Marchand, J. L. Daschbach, R. S. Smith, and B. D. Kay, *J. Phys. Chem. A* **115**, 6002 (2011).
- <sup>12</sup>V. F. McNeill, F. M. Geiger, T. Loerting, B. L. Trout, L. T. Molina, and M. J. Molina, *J. Phys. Chem. A* **111**, 6274 (2007).
- <sup>13</sup>M. Kondo, H. Kawanowa, Y. Gotoh, and R. Souda, *J. Chem. Phys.* **121**, 8589 (2004).
- <sup>14</sup>B. Henson, K. Wilson, J. Robinson, C. Noble, J. Casson, and D. Worsnop, *J. Chem. Phys.* **121**, 8486 (2004).
- <sup>15</sup>P. Parent and C. B. Laffon, *J. Phys. Chem. B* **109**, 1547 (2005).
- <sup>16</sup>S.-C. C. Park and H. Kang, *J. Phys. Chem. B* **109**, 5124 (2005).
- <sup>17</sup>J. Devlin, V. Buch, F. Mohamed, and M. Parrinello, *Chem. Phys. Lett.* **432**, 462 (2006).
- <sup>18</sup>N. Uras, V. Buch, and J. P. Devlin, *J. Phys. Chem. B* **104**, 9203 (2000).
- <sup>19</sup>C. Manca and A. Allouche, *J. Chem. Phys.* **114**, 4226 (2001).
- <sup>20</sup>Q. Chang and E. Herbst, *Astrophys. J.* **759**, 147 (2012).
- <sup>21</sup>A. Al-Halabi and E. F. Van Dishoeck, *Mon. Not. R. Astron. Soc.* **382**, 1648 (2007).
- <sup>22</sup>B. Barzel and O. Biham, *Astrophys. J. Lett.* **658**, L37 (2007).
- <sup>23</sup>M. E. Palumbo, *J. Phys.: Conf. Ser.* **6**, 211 (2005).
- <sup>24</sup>T. Huthwelker, M. Ammann, and T. Peter, *Chem. Rev.* **106**, 1375 (2006).
- <sup>25</sup>C. Girardet and C. Toubin, *Surf. Sci. Rep.* **44**, 159 (2001).

- <sup>26</sup>P. G. Sennikov, S. K. Ignatov, and O. Schrems, *ChemPhysChem* **6**, 392 (2005).
- <sup>27</sup>L. Amiaud, A. Momeni, F. Dulieu, J. Fillion, E. Matar, and J.-L. Lemaire, *Phys. Rev. Lett.* **100**, 056101 (2008).
- <sup>28</sup>J.-R. Li, R. Kuppler, and H.-C. Zhou, *Chem. Soc. Rev.* **38**, 1477 (2009).
- <sup>29</sup>A. Battisti, S. Taioli, and G. Garberoglio, *Microporous Mesoporous Mater.* **143**, 46 (2011).
- <sup>30</sup>G. Garberoglio, *EPJdirect* **51**, 185 (2009).
- <sup>31</sup>G. Garberoglio and J. Johnson, *ACS Nano* **4**, 1703 (2010).
- <sup>32</sup>H. Kagita, T. Ohba, T. Fujimori, H. Tanaka, K. Hata, S.-I. Taira, H. Kanoh, D. Minami, Y. Hattori, T. Itoh, H. Masu, M. Endo, and K. Kaneko, *J. Phys. Chem. C* **116**, 20918 (2012).
- <sup>33</sup>H. Tanaka, D. Noguchi, A. Yuzawa, T. Kodaira, H. Kanoh, and K. Kaneko, *J. Low Temp. Phys.* **157**, 352 (2009).
- <sup>34</sup>D. Liu, W. Wang, J. Mi, C. Zhong, Q. Yang, and D. Wu, *Ind. Eng. Chem. Res.* **51**, 434 (2012).
- <sup>35</sup>G. Garberoglio and R. Vallauri, *Microporous Mesoporous Mater.* **116**, 540 (2008).
- <sup>36</sup>W. L. Mao, H.-K. Mao, A. F. Goncharov, V. V. Struzhkin, Q. Guo, J. Hu, J. Shu, R. J. Hemley, M. Somayazulu, and Y. Zhao, *Science* **297**, 2247 (2002).
- <sup>37</sup>M. Xu, Y. S. Elmatad, F. Sebastianelli, J. W. Moskowitz, and Z. Bačić, *J. Phys. Chem. B* **110**, 24806 (2006).
- <sup>38</sup>F. Sebastianelli, M. Xu, Y. S. Elmatad, J. W. Moskowitz, and Z. Bačić, *J. Phys. Chem. C* **111**, 2497 (2007).
- <sup>39</sup>T. C. W. Mak and R. K. McMullan, *J. Chem. Phys.* **42**, 2732 (1965).
- <sup>40</sup>T. Castro, R. Reifengerger, E. Choi, and R. P. Andres, *Phys. Rev. B* **42**, 8548 (1990).
- <sup>41</sup>M. Schmidt, R. Kusche, B. von Issendorff, and H. Haberland, *Nature (London)* **393**, 238 (1998).
- <sup>42</sup>M. O'Keeffe, *Chem. Soc. Rev.* **38**, 1215 (2009).
- <sup>43</sup>L. J. Murray, M. Dinca, and J. R. Long, *Chem. Soc. Rev.* **38**, 1294 (2009).
- <sup>44</sup>I. Matanović, J. L. Belof, B. Space, K. Sillar, J. Sauer, J. Eckert, and Z. Bačić, *J. Chem. Phys.* **137**, 014701 (2012).
- <sup>45</sup>S. K. Pope, M. G. Tomasko, M. S. Williams, M. L. Perry, L. R. Dose, and P. H. Smith, *Icarus* **100**, 203 (1992).
- <sup>46</sup>M. E. Brown and W. M. Calvin, *Science* **287**, 107 (2000).
- <sup>47</sup>L. Slobodkin, I. Buyakov, R. Cess, and J. Caldwell, *J. Quant. Spectrosc. Radiat. Transf.* **20**, 481 (1978).
- <sup>48</sup>L. J. Lanzarotti, W. L. Brown, K. J. Marcantonio, and R. E. Johnson, *Nature (London)* **312**, 139 (1984).
- <sup>49</sup>M. J. Loeffler, U. Raut, and R. A. Baragiola, *J. Chem. Phys.* **132**, 054508 (2010).
- <sup>50</sup>J. He, K. Gao, G. Vidali, C. J. Bennett, and R. I. Kaiser, *Astrophys. J.* **721**, 1656 (2010).
- <sup>51</sup>G. Manic, G. Ragan, V. Pirronello, J. E. Roser, and G. Vidali, *Astrophys. J. Lett.* **548**, L253 (2001).
- <sup>52</sup>J. E. Roser, G. Manic, V. Pirronello, and G. Vidali, *Astrophys. J.* **581**, 276 (2002).
- <sup>53</sup>T. Hama, K. Kuwahata, N. Watanabe, A. Kouchi, Y. Kimura, T. Chigai, and V. Pirronello, *Astrophys. J.* **757**, 185 (2012).
- <sup>54</sup>M. Z. Kamrath, E. Garand, P. A. Jordan, C. M. Leavitt, A. B. Wolk, M. J. Van Stipdonk, S. J. Miller, and M. A. Johnson, *J. Am. Chem. Soc.* **133**, 6440 (2011).
- <sup>55</sup>J. G. L. C. A. Schmuttenmaer, R. C. Cohen, M. J. Elrod, D. W. Steyert, R. J. Saykally, R. E. Bumgarner, and G. A. Blake, *J. Chem. Phys.* **97**, 4727 (1992).
- <sup>56</sup>F. Huisken and T. Pertsch, *Chem. Phys.* **126**, 215 (1998).
- <sup>57</sup>B. Heijmen, A. Bizzarri, S. Stolte, and J. Reuss, *Chem. Phys.* **126**, 201 (1988).
- <sup>58</sup>U. Buck, R. Krohne, and S. Schoette, *J. Chem. Phys.* **106**, 109 (1997).
- <sup>59</sup>M. N. Slipchenko, B. G. Sartakov, A. F. Vilesov, and S. S. Xantheas, *J. Phys. Chem. A* **111**, 7460 (2007).
- <sup>60</sup>M. Patrone and M. Mella, *Chem. Phys. Lett.* **514**, 16 (2011).
- <sup>61</sup>S. Maret, A. Faure, E. Scifoni, and L. Wiesenfeld, *Mon. Not. R. Astron. Soc.* **399**, 425 (2009).
- <sup>62</sup>M. Mladenović, M. Lewerenz, G. Cilpa, P. Rosmus, and G. Chambaud, *Chem. Phys.* **346**, 237 (2008).
- <sup>63</sup>J. Sheppelman, Jr., G. Smizaski, E. Curotto, and M. Mella, *Chem. Phys. Lett.* **535**, 49 (2012).
- <sup>64</sup>P. Janeiro-Barral, M. Mella, and E. Curotto, *J. Phys. Chem. A* **112**, 2888 (2008).
- <sup>65</sup>T. Zeng, H. Li, R. J. L. Roy, and P.-N. Roy, *J. Chem. Phys.* **135**, 094304 (2011).
- <sup>66</sup>H. Li, P.-N. Roy, and R. J. L. Roy, *J. Chem. Phys.* **133**, 104305 (2010).
- <sup>67</sup>W. Kolos and L. Wolniewicz, *J. Chem. Phys.* **46**, 1426 (1967).
- <sup>68</sup>P. Slavicek and M. Lewerenz, *Phys. Chem. Chem. Phys.* **12**, 1152 (2010).
- <sup>69</sup>T. P. Straatsma and J. A. McCammon, *Mol. Simul.* **5**, 181 (1990).
- <sup>70</sup>C. Lubombo, E. Curotto, P. Janeiro Barral, and M. Mella, *J. Chem. Phys.* **131**, 034312 (2009).
- <sup>71</sup>E. Curotto and M. Mella, *J. Chem. Phys.* **133**, 214301 (2010).
- <sup>72</sup>P. E. Janeiro-Barral and M. Mella, *J. Phys. Chem. A* **110**, 11244 (2006).
- <sup>73</sup>B. Hartke, *J. Chem. Phys.* **97**, 9973 (1993).
- <sup>74</sup>Y. Zeiri, *Phys. Rev. E* **51**, R2769 (1995).
- <sup>75</sup>D. M. Deaven and K. M. Ho, *Phys. Rev. Lett.* **75**, 288–291 (1995).
- <sup>76</sup>D. M. Deaven, N. Tit, J. R. Morris, and K. M. Ho, *Chem. Phys. Lett.* **256**, 195 (1996).
- <sup>77</sup>J. A. Niesse and H. R. Mayne, *J. Chem. Phys.* **105**, 4700 (1996).
- <sup>78</sup>J. B. Anderson, *J. Chem. Phys.* **63**, 1499 (1975).
- <sup>79</sup>B. L. Hammond, W. A. Lester, and P. J. Reynolds, *Monte Carlo Methods in Ab Initio Quantum Chemistry* (World Scientific, Singapore, 1994).
- <sup>80</sup>M. Mella, *J. Chem. Phys.* **135**, 114504 (2011).
- <sup>81</sup>M. H. Kalos, *J. Comput. Phys.* **1**, 257 (1966).
- <sup>82</sup>V. Buch, P. Sandler, and J. Sadlej, *J. Phys. Chem. B* **102**, 8641 (1998).
- <sup>83</sup>M. Mella and D. C. Clary, *J. Chem. Phys.* **119**, 10048 (2003).
- <sup>84</sup>J. K. Gregory and D. C. Clary, *Chem. Phys. Lett.* **228**, 547 (1994).
- <sup>85</sup>E. Curotto, D. L. Freeman, and J. D. Doll, *J. Chem. Phys.* **128**, 204107 (2008).
- <sup>86</sup>M. Mella, J.-L. Kuo, D. C. Clary, and M. L. Klein, *Phys. Chem. Chem. Phys.* **7**, 2324 (2005).
- <sup>87</sup>M. Mella, G. Morosi, and D. Bressanini, *Phys. Rev. E* **61**, 2050 (2000).
- <sup>88</sup>S. Wolf and E. Curotto, *J. Chem. Phys.* **137**, 014109 (2012).
- <sup>89</sup>Q. Zhang, L. Chenyang, Y. Ma, F. Fish, M. M. Szcześniak, and V. Buch, *J. Chem. Phys.* **96**, 6039 (1992).
- <sup>90</sup>P. Valiron, M. Wernli, A. Faure, L. Wiesenfeld, C. Rist, S. Kedžuch, and J. Noga, *J. Chem. Phys.* **129**, 134306 (2008).
- <sup>91</sup>S. Patchkovskii, J. S. Tse, S. N. Yurchenko, L. Zhechkov, T. Heine, and G. Seifert, *Proc. Natl. Acad. Sci. U.S.A.* **102**, 10439 (2005).
- <sup>92</sup>O. Hübner, A. Glöss, M. Fichtner, and W. Klopper, *J. Phys. Chem. A* **108**, 3019 (2004).
- <sup>93</sup>B. Assfour, S. Leoni, S. Yurchenko, and G. Seifert, *Int. J. Hydrogen Energy* **36**, 6005 (2011).
- <sup>94</sup>A. Martínez-Mesa, L. Zhechkov, S. N. Yurchenko, T. Heine, G. Seifert, and J. Rubayo-Soneira, *J. Phys. Chem. C* **116**, 19543 (2012).